Kinetic Analysis of Cellular Internalization and Expulsion of Unstructured D-chirality Cell Penetrating Peptides

Manibarathi Vaithiyanathan[†], Hannah C. Hymel[†], Nora Safa[1†], Olivia M. Sanchez[†], Jacob H. Pettigrew[2†], Cole S. Kirkpatrick[3†], Ted J. Gauthier[‡], Adam T. Melvin[†]*

[†]Cain Department of Chemical Engineering, Louisiana State University, Baton Rouge, Louisiana 70803, United States

[‡]LSU AgCenter Biotechnology Lab, Louisiana State University, Baton Rouge, Louisiana 70803, United States

ABSTRACT: Most cell penetrating peptides (CPPs) are unstructured and susceptible to proteolytic degradation. One alternative is to incorporate D-chirality amino acids into unstructured CPPs to allow for enhanced uptake and intracellular stability. This work investigates CPP internalization using a series of time, concentration, temperature, and energy dependent studies, resulting in a three-fold increase in uptake and 50-fold increase in stability of D-chirality peptides over L-chirality counterparts. CPP internalization occurred via a combination of direct penetration and endocytosis, with a percentage of internalized CPP expelling from cells in a time-dependent manner. Mechanistic studies identified that cells exported the intact internalized D-chirality CPPs via an exocytosis independent pathway, analogous to a direct penetration method out of the cells. These findings highlight the potential of D-chirality CPPs as bio-vectors in therapeutic and biosensing applications, but also identify a new expulsion method suggesting a relationship between uptake kinetics, intracellular stability, and export kinetics.

Keywords: cell penetrating peptide, chirality, intracellular stability, direct penetration, export kinetics

INTRODUCTION

Cell-penetrating peptides (CPPs) are a class of short peptides (<30 amino acids) that penetrate intact biological membranes without compromising or rupturing them. In recent years, CPPs have become an important tool for the delivery of macromolecular cargoes inside cells. These sequences have found applications in targeted drug delivery and biosensing via conjugation with biomaterials, intracellular probes, anti-cancer therapeutics, small molecule inhibitors, and antimicrobial drugs.[1-3] Established CPPs like TAT (TAT-JBD20) and penetratin (PRX002) are currently being tested in preclinical and clinical trials. Novel CPPs like AZX100 (Capstone Therapeutics), RT001 (ReVance Therapeutics) and KAI-9803 (KAI Pharmaceuticals) are currently in clinical trials for keloid scarring and myocardial infarction.[4] CPPs have also found an important role in the development of novel therapeutic compounds called PROTACs (proteolysis targeting chimeras). PROTACs harness the naturally occurring ubiquitination machinery inside of the cells to target "undruggable" proteins such as ErbB3, FKBP12, and the Tau protein to the proteasome for degradation.[5-7] Besides therapeutics, CPPs have also been extensively exploited in the fields of biosensing and bioimaging. Gui and colleagues employed CPPs, particularly cyclic polyarginine (cR10), to deliver an activity-based deubiquitinating (DUB) reporter into cells which facilitated DUB profiling in intact HeLa cells.[8] Similarly, Safa et al. developed a β-hairpin CPP-based fluorescent bioreporter to screen for DUB activity in intact cancer cells.[9] The need for incorporating CPPs into biosensors has increased recently due to novel single cell analysis techniques. These high-throughput screening approaches have relied on electroporation and microinjection to introduce peptide-based reporters into single intact cells.[9-11] In addition to their application as inert vectors for intracellular delivery, an emerging dual-acting CPP technique is being studied which can function as both a membrane permeating component and a bioactive agent.[12]

Despite the vast potential of CPPs, one significant limitation is their rapid degradation in the presence of extracellular and intracellular enzymes. Most CPPs are unstructured sequences that are rapidly degraded by intracellular proteases and peptidases which consequently render these compounds less effective for *in vivo* or *in vitro* applications.[13-15] Several strategies have been employed to increase CPP stability such as the incorporation of non-natural amino acids, a pronounced secondary structure, or an increase backbone rigidity through macrocyclization.[16 17] Recent work by Safa et al. investigated the role of β-hairpin protectides as potential CPPs with enhanced intracellular stability.[18] Results from this study suggested that despite exhibiting lower cellular permeability than their unstructured versions, the β-hairpin CPPs had a ~15-fold increase in intracellular stability. One challenge associated with these strategies is that to increase intracellular peptide stability, uptake efficiency was compromised identifying a trade-off between peptide internalization efficiency and enhanced intracellular stability. To overcome this disadvantage, a chemical modification strategy was used in this work where a simple L-to-D chirality amino acid conversion was performed on previously characterized unstructured CPPs. D-chirality amino acids are non-natural and have been shown to be protease resistant.[19] Recent studies suggest that cellular uptake of CPPs is independent of backbone chirality, thus providing a possibility to preserve the permeability efficiency of previously described unstructured L-chirality CPPs.[18 20] This approach has been applied to other unstructured CPPs including TAT, R9, penetratin, hLF, pVEC, and sweet arrow peptide.[20-22] The extended *in vivo* half-lives of D-chirality CPPs over L-chirality CPPs have contributed to the successful development of the D-chirality polyarginine (R9) CPP as cancer contrast agents.[22] While new D-chirality CPPs are being synthesized and characterized, none of them have found success in the clinic due to the fact that the uptake mechanism has not been elucidated. In the case of unstructured, L-chirality CPPs,

uptake is known to occur via two major pathways: direct penetration or endocytosis (or a combination of both). While several intrinsic factors such as charge, hydrophobicity, structural composition and cellular composition regulate CPP uptake, role of chirality in uptake efficiency is still unclear.[23] The effect of chirality on endocytosis has been reported for the CPPs R9, penetratin, and hLF by Verdurmen et al.[24] Preferential uptake of L-chirality CPPs over D-chirality CPPs was observed, suggesting that chirality is important for the interactions between these compounds and cell-surface partners that induce endocytosis. Conversely, recent work by Najjar et al. showed that an L-to D-chirality conversion of dfTAT did not affect its cellular uptake mechanism or efficiency.[21] Together, these studies reveal conflicting results in predicting how L- to D-chirality amino acid substitutions affect to CPP-cellular interactions.

Several questions related to the effect of chirality on CPP uptake remain unanswered. In particular, how chirality impacts internalization and endosomal escape during the cell penetration process and how an unnatural D-chirality CPP alters cell physiology once inside a cell. The issue of endosomal escape is important because this step is critical for the successful delivery of molecules of interest into a cell via endocytosis. The goal of this work was to provide new insight into these questions by testing D-chirality versions (DS-rwrwr, DS-rwowr, DS-owrwr, Fig 1A) of previously reported unstructured, L-chirality CPP (S-RWRWR, S-RWOWR, S-OWRWR).[18] Degradation studies demonstrated a ~50-fold increase in half-life of DS-rwrwr against S-RWRWR in HeLa lysates. Time-dependent uptake studies revealed prominent cellular permeability of DS-rwrwr (~3-fold and ~100-fold increases compared to S-RWRWR and ARG, respectively) without negatively affecting cellular viability. These findings indicate that charge, hydrophobicity and chirality all regulate CPP uptake. While the majority of CPP uptake occurred via direct penetration, energy-dependent studies found that internalization was primarily regulated by direct penetration

and endocytosis to some extent. Interestingly, time-dependent degradation and export studies of DS-rwrwr found that despite negligible degradation, the amount of intact peptide diminished suggesting that it was exported out of cells through a direct penetration-like method instead of via exocytosis. A mathematical model suggested a maximum intracellular CPP concentration of 7.86 μM after 13.3 min of incubation which slowly decreased over time until a pseudo state of 5.45 μM was observed after 24 h. CPP internalization was accompanied by an export out of cells with an approximate extracellular CPP concentration of 3.14 μM after 24 h. These empirical and theoretical results establish the positive effect of an L-to D-chirality amino acid substitution in increased CPP permeability efficiency, intracellular stability, and cytosolic entry while elucidates a new finding on peptide export via an alternate route other than exocytosis.

MATERIALS AND METHODS

Chemicals and Reagents. Fmoc-protected amino acids, 2-(6-Chloro-1H-benzotriazole-1-yl)-1, -1,3,3-tetramethylaminium hexafluorophosphate (HCTU), trifluoroacetic acid (TFA), and rink amide SS resin were purchased from Advance ChemTech, Louisville, Kentucky. Nα-Fmoc-Nδ-allyloxyca bonyl-Lornithine (Fmoc-Orn[Aloc]-OH) was purchased from Chem-Impex International, Inc, Wood Dale, Illinois. 1-Hydroxy-6-(trifluoromethyl) benzotriazole (HOBt) and (Ethyl cyano[hydroxyimino]acetato)-tri-(1-pyrrolidinyl)-phosphonium (PyBOP) were purchased from Novabiochem, Billerica, Massachusetts. Dimethylformamide (DMF) was purchased from Protein Technologies, Tucson, Arizona. Diisopropylethylamine (DIEA), triisopropylsilane (TIPS), tetrakis(triphenylphosphine) palladium (0) (palladium), 5(6)-carboxyfluorescein (FAM), chloroform (CHCl3), methanol (MeOH), dichloromethane (DCM), and N-methylmorpholine (NMM) were purchased from Sigma-Aldrich, St. Louis, Missouri. Glacial acetic acid was purchased from Alfa Aesar, Ward Hill, Massachusetts. Acetic anhydride was purchased from

Fisher Scientific, Fair Lawn, New Jersey. Commercial peptides TAT (FAM-YGRKKRRQRRR) and ARG (FAM-RRRRRRRRR)] were purchased from AnaSpec, Fremont, California. All the salts used for the preparation of assay buffers were purchased from Sigma Aldrich, St. Louis, Missouri.

Peptide Synthesis and Purification. The steps involved in the synthesis and purification of L- and D-chirality peptides are explained in detail in Supplementary Information, Section Peptide Synthesis and Purification. Representative data for the HPLC purification and mass spectrometry validation of the DS-rwrwr peptide are presented in Supporting Information, Fig S1.

Cell Culture and Lysate Generation. HeLa cells (LSU AgCenter Tissue Culture Facility) were maintained in Dulbecco's modified eagle medium (DMEM, Corning) supplemented with 10% v/v HyClone Cosmic Calf Serum (VWR Life Sciences Seradigm). HeLa lysates were generated by harvesting 1 x 10^6 cells/mL, followed by washing 2x and pelleting in 1X phosphate buffered saline, PBS (137 mM NaCl, 10 mM Na_2HPO_4, 27 mM KCl, and 1.75 mM KH_2PO_4 at pH 7.4). The cell pellet was then resuspended in an approximately equivalent volume of M-PER mammalian protein extraction reagent (ThermoFisher Scientific, Carlsbad, CA, USA) to the volume of the cell pellet (~1000-2000 μL) then vortexed for 10 minutes at 900 rcf at room temperature. Following this, the mixture was centrifuged at 14,000 rcf for 15 minutes at 4°C and the supernatant transferred to a centrifuge tube and stored on ice until use. Total protein concentration was estimated by near-UV absorbance A_{280} using a NanoDrop spectrophotometer (Thermo Scientific, Madison, WI, USA) with M-PER mammalian protein extract reagent as background control.

Circular Dichroism. For all the experiments described henceforth, the peptides were reconstituted in 10 mM sodium phosphate buffer (2.26 mM $NaH_2PO_4 \cdot H_2O$ and 8.43 mM $Na_2HPO_4 \cdot 7H_2O$, pH 8.02). Stock peptide concentration was determined using a NanoDrop spectrophotometer (Thermo

Scientific, Madison, WI, USA) at the wavelength of 492 nm using the UV-vis function. For this experiment, all peptides were at a final concentration of 40 μM in 10 mM sodium phosphate buffer. Circular dichroism (CD) spectroscopy data were collected using a J-815 CD spectrometer (JASCO, Easton, MD, USA). Spectra were generated at 25°C with a wavelength scan (260-185 nm) using 50 nm/min scanning speed in a 0.1 cm cell. Data pitch and accumulation were 1 and 3 nm, respectively. Scan mode was continuous. The smoothing method was Savitzky-Golay with a convolution width of 7.

Peptide Degradation Assay. Briefly, 30 μM of respective peptide was incubated in HeLa lysates diluted to a total protein concentration of 2 mg/mL in an assay buffer (10 mM sodium phosphate buffer, 100 mM NaCl, pH 7.6) at 37°C in the dark. Aliquots of the reaction mixture were removed at set intervals, at which point further peptidase activity was quenched by heating the aliquots at 90°C for 5 minutes followed by immediately freezing in liquid nitrogen and then storage at −20°C until analysis by HPLC. The zero-minute time point measurements were made using lysates that were heat killed immediately after peptide incubation. HPLC analysis was performed with a Waters 616 pump, Waters 2707 Autosampler, and 996 Photodiode Assay Detector which are controlled by Waters Empower 2 software. The separation was performed on an Agilent Zorbax 300SB-C18 (5 μm, 4.6 × 250 mm) with an Agilent guard column Zorbax 300SB-C18 (5 μm, 4.6 × 12.5 mm). Elution was done with a linear 5%-85% gradient of solvent B (0.1% TFA in acetonitrile) into A (0.1% TFA in water) over 40 minutes at 40 μL injection volume and a 1 mL/min flow rate with UV detection at 445 nm. Sample chromatograms for DS-rwrwr and S-RWRWR can be seen in Supporting Information, Fig S2 and in the previous work. Peak areas were calculated by the Waters Empower 2 software by integration of peaks identified using a peak width of 30.00 and a peak threshold of 50.00. Percent intact peptide remaining was calculated by

dividing the area of the parent peptide peak at each time point divided by the area of the parent peptide peak at the zero-minute time point. The identity of the parent peptide peak was confirmed using the parent peptide alone and verified with the t = 0-minute chromatogram. Experiments were performed twice to ensure reproducibility.

Quantification of Cellular Peptide Uptake. Three days prior to the experiment, HeLa cells were seeded in 12-well plates (Corning) at a density of $1x10^4$ cells/mL with 1 mL in each well. On the day of experiment, peptides were diluted to the desired final concentrations in extracellular buffer, ECB (5.036 mM HEPES pH 7.4, 136.89 mM NaCl, 2.68 mM KCl, 2.066 mM $MgCl_2•6H_2O$, 1.8 mM $CaCl_2•2H_2O$, and 5.55 mM glucose). The cells were washed 1x with 1X PBS (1 mL/well) followed by peptide incubation (500 µL/well) for desired time points or under different conditions. The different conditions were based on time-, concentration-, temperature- and energy-dependent characterization. For time dependent studies, 10 µM of peptide solutions in ECB were incubated with HeLa cells for different incubation times (10, 20, 40, 60, 100 and 120 min) over a span of 2 hours at 37°C. For concentration dependent studies, four different concentrations (5, 10, 20 and 30 µM) of peptide solutions in ECB were incubated with HeLa cells for 60 min at 37°C. For temperature dependent studies, cellular uptake at 37°C was compared with uptake at 4°C. Similarly, the effects of 5% serum and endocytosis inhibitors (10 mM sodium azide + 5 mM 2-deoxyglucose, Sigma Aldrich) on peptide uptake were evaluated in case of energy dependent studies. For these temperature and energy-sensitive experiments, the cells were pretreated for 2 h before experimentation and constantly exposed to these conditions throughout experimentation (e.g., wash steps and peptide incubation) to maintain experimental consistency.

During peptide incubation, all plates were wrapped in aluminum foil to avoid deactivating the FAM tag on the peptide. Following the incubation, the peptide solution was removed, and the cells

were washed 2x with ECB (1 mL/well) to remove any membrane-bound peptide debris. The cells were trypsinized (200 μL/well) for 10 min at room temperature to detach the cells from the wells and remove any remaining peptide adhered to the extracellular surface. The cells were then re-suspended in ECB (1 mL/well), thoroughly mixed, and transferred to microcentrifuge tubes. The samples were centrifuged (1800 rcf, 2.5 min, at room temperature) to isolate the cells. Following centrifugation, the supernatant was discarded, and the pellet was lysed with 0.1 M NaOH (250 μL/tube). While the fluorescence intensity of FAM has been demonstrated to be dependent on pH, it was confirmed by Safa et al. that the 0.1 M NaOH had negligible effects on the intensity profile of CPPs at both 10 μM and 30 μM concentrations.[18] Each sample was then transferred to a 96-well plate and quantified by fluorometry (Perkin Elmer (Waltham, MA) Wallac 1420 VICTOR2 multilabel HTS counter). The FAM tag was quantified using an excitation filter of 490 nm and an emission filter of 535 nm. During every experiment, a no peptide control was performed (e.g., cells incubated with ECB only). To measure the background signal of each peptide, the peptide solutions used in each experiment were analyzed by fluorometry to normalize the observed fluorescent signal for each sample. This allowed for an unbiased comparison between different peptides used in this study. The fluorescent signal measured by the plate reader was normalized using Equation (1):

$$Normalized\ Fluorescence = 1000\ X\ \frac{(F-C)}{(P-B)} \quad \text{(Eq. 1)}$$

where, F denotes the fluorescent signal of cells incubated with peptide, C denotes the fluorescent signal of cells incubated with no peptide, P denotes the average fluorescent signal of the peptide in suspension, and B denotes the average fluorescent signal of the ECB. Data reported for each peptide are the average of triplicate samples. Standard deviations were calculated based on the triplicate samples to obtain the error bars and perform analysis of variance. Each experiment was

repeated twice to ensure reproducibility. All time-, concentration-, temperature- and energy-dependent uptake characterization experiments were performed in serum-free media unless otherwise noted.

Characterization of Cellular Peptide Export. A modified version of the experimental protocol was performed to study peptide export from cells after internalization. To accomplish this, 10 μM of peptide solution was incubated with intact HeLa cells seeded on 12-well plates for 10 min at 37°C in the dark. After this 10-min incubation period, the peptide solution was removed, and the cells were washed 2x with ECB. Fresh ECB was added to the cells which were further incubated in the dark for indicated incubation times (0, 10, 20, 40, 60, 100, 120, 150 min) to study peptide export rates. After the indicated timepoints, the cells were trypsinized, lysed, and transferred to a 96-well plate for fluorescence measurements using the steps as previously described. Samples that were lysed immediately after peptide removal were marked as the zero-min time point in terms of peptide export. Cellular peptide export was evaluated under three different energy-dependent conditions: presence and absence of 5% serum and exocytosis inhibitor, Exo-1 (Sigma Aldrich) at 37°C. For this, the cells were pretreated for 2 h before experimentation and the cells were constantly exposed to these conditions during the 10-min peptide incubation, wash steps and ECB incubation in order to maintain consistency. All experimentation conditions were performed in triplicate with every experiment performed twice to ensure reproducibility. All export characterization experiments were performed in serum-free media unless otherwise noted.

Fluorescence Microscopy and Image Analysis. Two days prior to the experiment, HeLa cells were seeded in 8-chambered Falcon Culture Slides (Corning) at a density of $1x10^4$ cells/mL with 500 μL in each chamber. On the day of experimentation, the culture media was removed, and the cells were then washed 1x with 1X PBS. A total of 500 μL of peptide solution in ECB was

incubated with HeLa cells for different time periods at different conditions in the dark. After the incubation period, the peptide solution was removed, and the cells were washed 2x with ECB to remove excess, unbound peptides. Cells were then fixed with 4% paraformaldehyde (PFA) in 1X PBS for 10 min. Post fixing, the cells were incubated with 8 μM Hoechst 3342 nuclei acid stain for 30 min. To test viability, the cells were incubated with 10 μM and 30 μM DS-rwrwr in ECB for 5 h in the dark followed by washing 2x with ECB and staining with 4.5 μM EthD-1 for 30 min at 37°C in the dark before fluorescence microscopy imaging.

For imaging, cellular fluorescence was visualized using a Leica DMi8 inverted microscope outfitted with a fluorescein isothiocyanate (FITC: λ_{ex}: 440–520 nm and λ_{em} = 497–557 nm) filter cube, 10× and 20× objectives (Leica HC PL FLL, 0.4× correction), and phase contrast and brightfield applications. Cellular viability and nucleic acid staining were observed with Rhodamine (λ_{ex} 536–556 nm and λ_{em} 545–625 nm) and DAPI (λ_{ex} 335–385 nm and λ_{em} 405–465 nm) filters. Digital images were acquired using the Flash 4.0 high speed camera (Hamamatsu) with a fixed exposure time of 500 ms for FITC, 40 ms for DAPI, and 200 ms for Rhodamine filters, and 30 ms for brightfield. Image acquisition was controlled using the Leica Application Suite software. All images were recorded using the same parameters. All data visualization and interpretation were performed using Origin Pro (OriginLab, Northampton, MA) while statistical analyses of experimental data were carried out using SAS 9.4 (SAS Solutions).

Mathematical Modeling. Data obtained from time-dependent uptake, degradation and export experiments executed with DS-rwrwr were used to determine the rate constants using MATLAB, R2017a. The steps involved in modeling rate kinetics for each step using non-linear curve fitting and regression analyses are explained in detail in Supplementary Information, Section Mathematical Modeling.

A)

Name	Sequence
DS-rwrwr	Ac-**r**wv**r**wiO(FAM)qv**r**pg-NH_2
DS-rwowr	Ac-**r**wv**o**wiO(FAM)qv**r**pg-NH_2
DS-owrwr	Ac-**o**wv**r**wiO(FAM)qv**r**pg-NH_2
S-RWRWR	Ac-**R**WV**R**WIO(FAM)QV**R**pG-NH_2
S-RWOWR	Ac-**R**WV**O**WIO(FAM)QV**R**pG-NH_2
S-OWRWR	Ac-**O**WV**R**WIO(FAM)QV**R**pG-NH_2
III-67B	FAM-GGAYAAPFKKKA-NH_2
TAT	(5-FAM)-YGRKKRRQRRR-OH
ARG	(5-FAM)-RRRRRRRRR-OH

B)

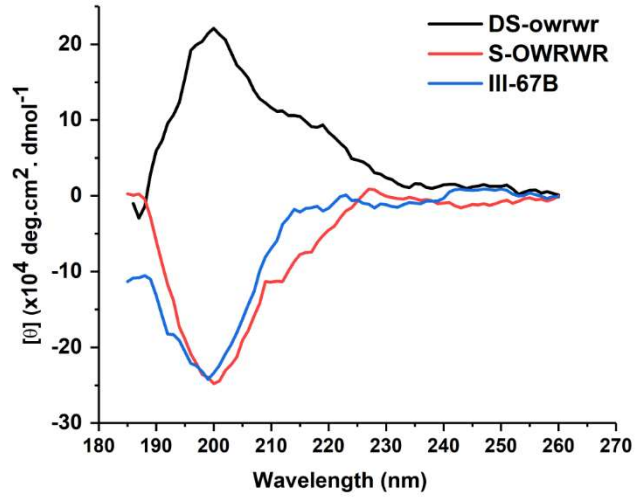

C)

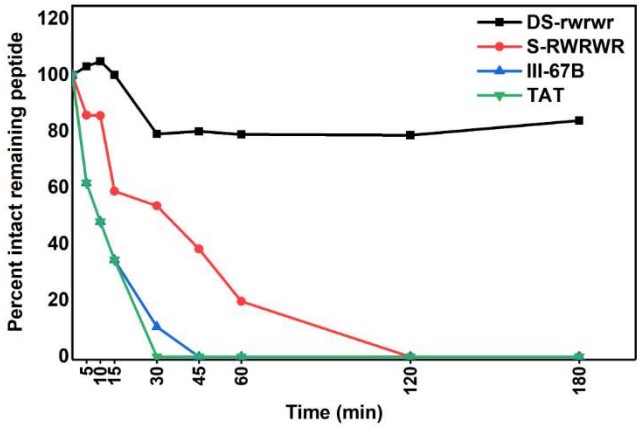

Fig 1. Stability of D-chirality peptides in HeLa cells. *(A) Names and sequences of peptides studied. Bold amino acids (O/o-ornithine, R/r-arginine) at positions 1, 4, and 11 were altered for different library members. Substrates were acetylated at the N-terminus and amidated at the C-terminus. FAM denotes 5,6-carboxyfluorescein. Scrambled, D-chirality peptides are denoted by a "DS", while the L-chirality versions are denoted by an "S" in the name. (B) CD spectra of D-chirality and L-chirality peptides. Experiments were performed using 40 μM peptide solution in 10 mM sodium phosphate buffer, pH 8.02 at 25°C. The DS-owrwr peptide (black) exhibited a D-chirality spectrum based on the maximum near 200 nm. Conversely the S-OWRWR (red) and III67B (blue) peptides were determined to be unstructured with an L-chirality based on the minimum near 198 nm.* (C) *The stability of the D-chirality, L-chirality, and commercially available peptides was evaluated by incubation with 2 mg/mL HeLa lysates at 37°C. The D-chirality peptide DS-rwrwr (black squares, $t_{1/2}$ = 1550 minutes) was substantially more resistant to degradation than its L-chirality counterpart S-RWRWR (red circles, $t_{1/2}$ = 28 minutes) as evidenced by a substantially greater amount of intact peptide and a significantly higher half-life. The commercially available TAT peptide exhibited rapid degradation in the HeLa lysates (inverted green triangles, $t_{1/2}$ = 10.0 min). An unstructured, rapidly degraded peptide (III-67B) was used as a positive control to demonstrate the activity of the HeLa lysates (blue triangles, $t_{1/2}$ = 9.5 minutes).*

RESULTS AND DISCUSSION

D-chirality Amino Acid Substitutions in a CPP Enhance Peptide Proteolytic Stability.

Chemical modification by incorporating D-chirality amino acids have been performed on CPPs to

improve their stability against intracellular enzymes or serum.[22 25 26] To explore and understand the contribution of such a modification, a library of D-chirality, unstructured CPPs were synthesized (Fig 1A) by changing the chirality of three unstructured, scrambled sequences previously published by Safa et al.[18] Three D-chirality variants (DS-rwrwr, DS-rwowr, and DS-owrwr) were obtained by substituting D-ornithine for D-arginine at positions 1, 4 and 11. Arginine was used for its cationic property and ornithine for greater stability. Tryptophan and valine were incorporated in these sequences for their increased hydrophobicity. Circular dichroism (CD) was used to confirm the intrinsic structures of the synthesized D-chirality and L-chirality CPPs compared to an unstructured, non-permeable negative control (III67B peptide). The CD spectra of the S-OWRWR and III-67B confirmed that they were unstructured with L-chirality based on a minimum near 198 nm (Fig 1B, red and blue lines) while the DS-owrwr exhibited a maximum near 200 nm (Fig 1B, black line). The spectra show an exact mirror image when modified with opposite chirality and displays the well-known Cotton effect. This trend is consistent with the CD spectrum of previously published CPPs D-Phe-OEt, MoS2/D-Penicillamine, and D-SAP which have been well characterized using both NMR and CD for their D-chirality sequences.[22 27 28]

The stability of the synthesized peptides was investigated through a degradation assay. Select peptides were incubated with HeLa lysates to mimic the intracellular environment. The data points for percentage intact parent peptide over time was fit into a first-order exponential decay curve to determine half-lives of the intact peptides. As expected, the DS-rwrwr peptide was resistant to degradation in HeLa lysates (Fig 1C, black squares) with ~80% peptide remaining after 180 min and yielding a half-life of 1550 min. Conversely, the S-RWRWR peptide was mostly degraded within 120 min (Fig 1C, red circles) with a calculated half-life of 28 min. Thus, the chemical substitution of L-to D-chirality amino acids in DS-rwrwr resulted in an increase in stability with a

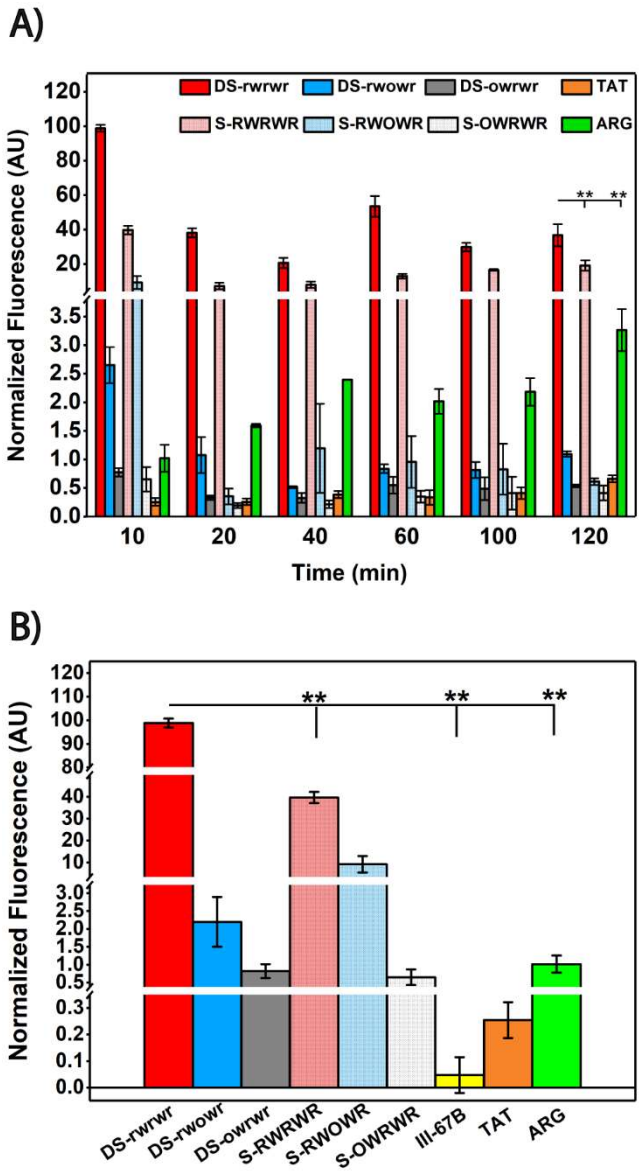

Fig 2. Time-dependent internalization of D-chirality peptides in HeLa cells *(A) Comparison of cell permeability in D-chirality peptides with L-chirality CPPs, and two commercially available L-chirality CPPs ARG and TAT. Intact HeLa cells were incubated with 10 μM peptide solutions for varying periods of time followed by lysis and quantification by fluorometry. Data demonstrates a significant effect of incubation time in cellular association of DS-rwrwr versus its L-chirality counterpart and ARG until 120 min. (B) Comparison of cellular uptake of all peptides at 10 min, with DS-rwrwr exhibiting the maximum uptake of ~100-fold increase over ARG. **denotes $p < 0.001$ for D-chirality peptides as compared to the L-chirality versions, III67B, and ARG to ensure the statistical significance of high performance of the D-chirality peptide. All data are representative of duplicate experiments with each data point performed in triplicate to produce the error bars.*

~50-fold increase in CPP half-life. A comparison with the well-known L-chirality TAT CPP found a mostly degraded peptide within 30 min (Fig 1C, inverted green triangles) with a calculated half-

life of 10 min. The stability of these three CPPs was compared to a non-permeable, negative control peptide (III-67B) which was previously demonstrated to rapidly degrade under cytosolic conditions exhibiting a half-life of 9.5 min (Fig 1C, blue triangles). The results obtained here for S-RWRWR, TAT and III-67B matched the previous study by Safa et al. while also revealing a ~3.5-fold increase in the half-life of the DS-rwrwr when compared to the β-hairpin RWRWR (423 min) under cytosolic conditions.[18] These findings indicate that an L-to D-chirality amino acid substitution in a CPP increases its stability under cytosolic conditions. They are also consistent with the previous observations for stable CPPs using D-amino acids, cyclic and secondary structures.[16 20]

L- to D-chirality Amino Acid Substitution in Unstructured CPPs Enhance Cellular Uptake. Modifying a CPP sequence to enhance intracellular stability can significantly alter its cellular uptake. This was previously seen with the ~5-fold decrease in the uptake of S-RWRWR when a secondary β-hairpin structure was incorporated to its sequence.[18] Previous works by Verdurmen et al., Najjar et al., and Pujals et al. have reported an increase in the cellular uptake of L-TAT and L-SAP peptides upon altering the chirality of their amino acids.[21 22 24] To further investigate the relationship between chirality and cellular uptake, the internalization of six unstructured CPPs (three D-chirality: DS-rwrwr, DS-rwowr, DS-owrwr and three L-chirality: S-RWRWR, S-RWOWR, S-OWRWR) was assessed in intact HeLa cells in a time-dependent manner (Fig 2A). Statistical t-tests and ANOVA F-tests were performed at each time point to illustrate the significance of observed intracellular fluorescent signals. The resultant data from Fig 2A and F-statistics from Supporting Information, Table S1 demonstrate a significant time-dependent uptake for all six peptides with maximum internalization occurring at 10 min coupled with a sharp decrease at 20 min followed by a steady internalization for the subsequent 100 min. The observed

oscillatory uptake kinetics for the D-chirality CPPs was attributed to the cells' tendency to equilibrate between a constant peptide source and export from cells when saturated with a maximum intracellular concentration. Cellular saturation was observed for L- chirality CPPs within the first 10 min followed by a gradual decrease in intracellular fluorescence due to their poor half-lives and intracellular degradation over time (Fig 1C). Contrary to this, a slow time-dependent increase in peptide internalization was observed for the two commercial CPPs (TAT: FAM-YGRKKRRQRRR and ARG: FAM-RRRRRRRRR) with maximum uptake only at 120 min.

To understand the performance of the D-chirality peptides, their cellular uptake was compared against their unstructured L-chirality counterparts, commercial peptides, and a non-permeable negative control III-67B at a single incubation time. Quantification of intracellular fluorescent signals at 10 min (Fig 2B) revealed that DS-rwrwr demonstrated the highest permeability followed by DS-rwowr (40-fold lower signal) and DS-owrwr (100-fold lower signal). This sequence-based ranking was observed within the L-chirality counterparts as well (S-RWRWR being the highest followed by S-RWOWR and S-OWRWR), highlighting the role of charge and amino acid position in peptide uptake. The additional arginine residue in DS-rwrwr/S-RWRWR (net total of three) and the position of the ornithine residue in DS-rwowr/S-RWOWR favors each of their uptake when compared to DS-owrwr/S-OWRWR. At the 10-min time point, DS-rwrwr demonstrated a ~3-fold increase in peptide uptake against S-RWRWR ($p<0.05$), clearly emphasizing the effect of L-to-D-chirality amino acid substitution on peptide uptake. Interestingly, the other two D-chirality CPPs demonstrated similar intracellular uptake levels as that of their L-chirality counterparts suggesting that the charge and position of select amino acid residues are just as important as chirality on CPP uptake. The DS-rwrwr peptide exhibited a ~100- and ~1000-fold increase against ARG ($p<0.001$) and III-67B ($p<0.0001$) respectively. Despite being highly cationic in nature and unstructured like

the L-chirality and D-chirality CPPs, the visibly slower and diminished uptake of ARG can attributed to its lower hydrophobicity. At 120 min, during an approximate steady state of peptide internalization, DS-rwrwr remained the best performer with a ~2- and ~10-fold increase against S-RWRWR ($p<0.005$) and ARG ($p<0.001$). These findings provide strong evidence for increased peptide internalization through an L-to D-chirality amino acid substitution in addition to the effect of charge, position and hydrophobicity in cellular uptake. The rapid and pronounced uptake of DS-rwrwr leading towards steady-state internalization coupled with greater intracellular stability signifies its utility as a replacement for existing commercial CPPs in designing therapeutics.

Initial Peptide Concentration Demonstrates a Significant Effect on the Permeability Efficiency of the D-CPPs without Negatively Affecting Cellular Viability. An important trait of any CPP is to avoid cytotoxicity which can be problematic with non-natural amino acids and

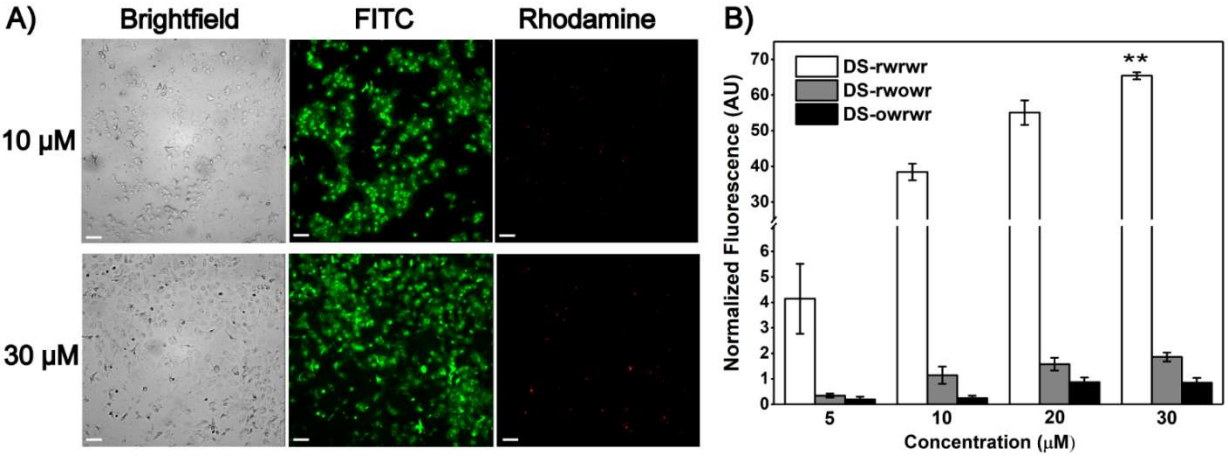

Fig 3. Concentration dependent internalization of D-chirality peptides and its effect on HeLa cells*. (A) Cellular viability of D-chirality peptides in HeLa cells. Intact HeLa cells were incubated with DS-rwrwr for 5 h at 37°C in dark followed by washing them with ECB before staining with 4 µM ethidium homodimer-1 (ethD-1) prior to imaging. Top row illustrates cells incubated with 10 µM of DS-rwrwr and bottom row depicts cells with 30 µM of DS-rwrwr. Signal in FITC denotes peptide uptake and no signal in Rhodamine denotes absence of dead cells. Ruptured cell membranes and DNA of dead cells stained in red by ethD-1. Representative images include brightfield, FITC (for peptide uptake), rhodamine (ethD-1-dead cells). All scale bars are 100 µm. (B) D-chirality peptides DS-rwrwr, DS-rwowr and DS-owrwr were incubated at mentioned concentrations for 60 min in intact HeLa cells followed by lysis and quantification by fluorometry. A strong concentration dependence is observed for DS-rwrwr and DS-rwowr. rhodamine (ethD-1-dead cells). ** denotes $p < 0.001$ for significant concentration dependent internalization of DS-rwrwr at 30 µM. All data are representative of duplicate experiments with each data point performed in triplicate to produce the error bars.*

their possibility for intracellular aggregation. A minimal toxic effect could potentially cause cell damage at the beginning of the treatment but would continue to exert this toxic effect until the peptide is eliminated. To investigate this possibility with the D-chirality CPPs, concentration-dependent cellular uptake of D-chirality CPPs and its effect on cellular viability were studied using fluorometry and fluorescence microscopy. Live cell microscopy results (Fig 3A and Supporting Information, Fig S3) show uniform intracellular peptide distribution in intact cells while preserving cellular morphology. A homogeneous intracellular distribution in the cytoplasm and nucleus was observed for all D-chirality CPPs without any membrane bound peptide debris. A negative control was performed by incubating the cells with only ECB (no peptide) to confirm the intracellular fluorescence was due to the CPPs (Supporting Information, Fig S3). The presence of few dead cells (~30 out of 210 cells) for both DS-rwrwr incubation (Fig 3A, Rhodamine) and no peptide incubation (Supporting Information Fig S3, Rhodamine) confirmed the viability of cells after peptide incubation at concentrations as high as 30 μM. It was suspected that the loss of viability in a small percentage of cells in both peptide-containing and peptide-free solutions was due to an extended incubation in ECB in the absence of serum. A positive control for EthD-1 indication of dead cells (Supporting Information, Fig S3) was done to validate the experiment protocol, where heat-shocked cells stained positive in the Rhodamine filter confirming dead cells.

The effect of initial concentration on CPP uptake was assessed upon confirming the viability of cells at relative concentrations. As shown in Fig 3B, there was a marked increase in peptide uptake for all three D-chirality CPPs when incubated with higher initial concentrations (>5 μM) compared to cells incubated with lower concentrations (<5 μM). Statistical analysis of peptide uptake found that initial concentration does have a significant effect on the permeability efficiency, though to variable extents across the different CPPs (Supporting Information, Table S2). The effect of

concentration was dramatic for DS-rwrwr which contains three arginine residues, exhibiting a significant increase in cellular uptake for increasing peptide concentrations ($p < 0.001$, Supporting Information Table S2). The linear dependence of DS-rwrwr with initial concentration reveals information about the mode of peptide entry. Studies have shown that cellular uptake of arginine rich CPPs at concentrations <10 μM occurs via endocytosis and direct penetration while transduction becomes a dominating uptake mode at concentrations >10 μM, resulting in greater internalized concentrations.[29] This trend was observed for arginine rich peptides like S-RWRWR, TAT and ARG as described in the previous work.[18] The effect of peptide concentration on the permeability efficiency was found to be weak and statistically insignificant for the DS-rwowr and DS-owrwr CPPs ($p>0.05$, Supporting Information Table S2) within the experimental concentration range of 10-30 μM. Thus, it was concluded that the uptake of DS-rwowr and DS-owrwr peptide did not change significantly by increasing the incubation concentration above 10 μM. This suggested that the substitution of an ornithine residue in place of the third arginine residue, irrespective of its position (at positions 1 or 4), affected the concentration-dependent uptake within the experimental range. Since incubation with a 10 μM peptide solution was experimentally sufficient to generate a statistically significant result, this concentration was used for the subsequent studies investigating DS-rwrwr uptake.

D-Chirality CPPs Exhibit Diminished Cellular Uptake in the Presence of Serum. Cell penetrating peptides have been successfully utilized for several *in vitro* and *in vivo* diagnostic applications like molecular imaging and targeted therapeutics.[30 31] In order to explore the utility of the D-chirality CPPs in *in vivo* applications, the effects of serum on time-dependent CPP uptake was studied. Intact HeLa cells were pretreated with media containing 5% calf serum for 2 h to mimic *in vivo* conditions, while a control population was pretreated with serum free media (SFM).

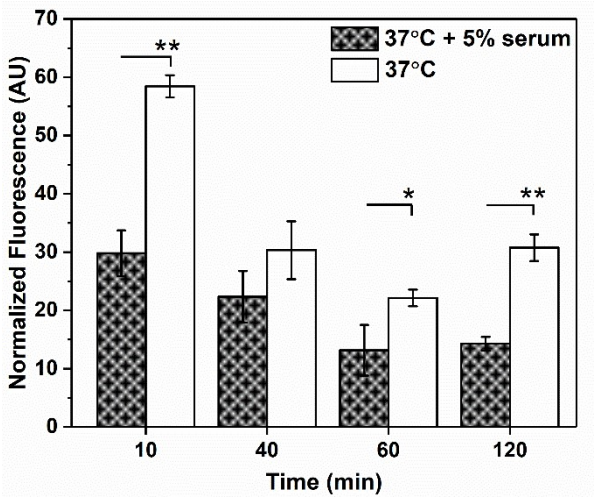

Fig 4. Effect of serum on peptide internalization in HeLa cells*. The intact cells were pretreated with 5% serum and serum free conditions for 2 h at 37°C before incubated them with 10 μM of DS-rwrwr with 5% serum and serum free media at 37°C in the dark for different time points. The cells were then washed with ECB, lysed and quantified for intracellular fluorescence by fluorometry. Peptide internalized decreased statistically in the presence of serum. *denotes $p < 0.05$ and **denotes $p < 0.001$ denotes statistical significance for decreased D-rwrwr uptake in the presence of serum when compared to serum free media. All data are representative of duplicate experiments with each data point performed in triplicate to produce the error bars.*

Time-dependent fluorometric measurements revealed that the presence of serum diminished the time-dependent uptake of DS-rwrwr in HeLa cells in a statistically significant manner (Fig 4 and Supporting Information, Table S3). The reduced initial cellular uptake in the presence of serum at 10 min, which was earlier shown to be the incubation time required for maximum internalization (Fig 2), suggests that serum inhibits peptide uptake. Cellular uptake in the presence of serum remained significantly lower than that of the serum-free condition throughout the 120-min incubation period ($p<0.001$, Supporting Information, Tables S3, S4). However, in the presence of serum, peptide internalization followed a similar oscillatory trend as was observed for D-chirality CPP uptake under serum-free conditions (Fig 2). Peptide uptake was observed to reach a pseudo-steady state after a 40 min incubation time. This suggested that while the presence of serum decreased overall CPP uptake, it did not alter the uptake mechanism but only reduced overall CPP permeability. One possible explanation is the formation of a protein corona around CPPs reducing their membrane adsorption and limiting their interaction with the membrane diminishing cellular

entry. Another possible explanation can be that serum components can decrease the zeta potential of positively charged CPPs. Previous study by Smith et al. revealed the reduced zeta potential of polystyrene nanoparticles in the presence of serum.[32] However, it is interesting to note that despite an observed reduction in permeability, DS-rwrwr uptake at 120 min in the presence of serum was still ~10-fold and ~3-fold higher than that of TAT and ARG (Fig 2).

The Limiting Mechanism for the Uptake of D-chirality CPPs Follows the Direct Penetration Model. Different mechanisms have been suggested for the cellular entry of CPPs depending upon the particular cell line used and/or the physiochemical characteristics of the specific peptides being tested (e.g., size, composition, concentration).[15 33] High molecular weight cargos (larger than 30,000 Da) including nanocarriers or proteins conjugated to CPPs are delivered intracellularly through phagocytosis.[34] However, the entry mechanism of small, low molecular weight CPPs (fewer than 50 amino acids) is controversial topic since it has the potential to involve different cellular pathways.[35] Preliminary studies by Holm et al. ~10 years ago found that Antp, R9, and TAT peptides simultaneously used three endocytic pathways: macropinocytosis, clathrin-mediated endocytosis, and caveolae/lipid raft-mediated endocytosis.[36] In contrast, recent work by Patel et al. on sequence dependent CPP uptake showed that cationic peptides like TAT and R9 shared commonalities of both endocytic as well as direct mechanisms of uptake.[37] Additionally, several recent studies have been published stating that internalization strongly depends on the peptide concentration with the direct penetration model being the most probable at high CPP concentrations (>5 μM).[14 15 33 38] Therefore, it was important to empirically determine which uptake mechanism might be involved in the entry of the cationic, ~3.5 nm-sized DS-rwrwr peptide at an external concentration of 10 μM in HeLa cells.

The transport of DS-rwrwr into cells was measured at either 37 ºC or 4 ºC to investigate if peptide uptake was energy independent (direct penetration) or energy dependent (endocytosis). A clear reduction of intracellular accumulation of DS-rwrwr was found after a 10 min incubation at 4°C when compared to experiments performed at 37°C (Fig 5). A similar decrease in peptide uptake was observed across the population of cells pretreated with two endocytosis inhibitors at 4ºC: 10 mM sodium azide (SA) + 5mM 2-deoxyglucose (2DG). SA and 2DG inhibit respiration and the glycolytic pathway, depleting the cells of ATP. Statistical analysis revealed that the peptide uptake at 4°C after a 10 min incubation in the presence of metabolic inhibitors was ~5-fold lower to that of cells incubated at 37°C ($p<0.001$, Supporting Information, Tables S3, S4). This suggested that cellular uptake of DS-rwrwr is energy dependent to some extent. As previously discussed for cells incubated with CPPs at 37°C, a saturation can occur with respect to peptide internalization within 10 min which slowly reached a pseudo steady state for uptake after 60 min. However, for the

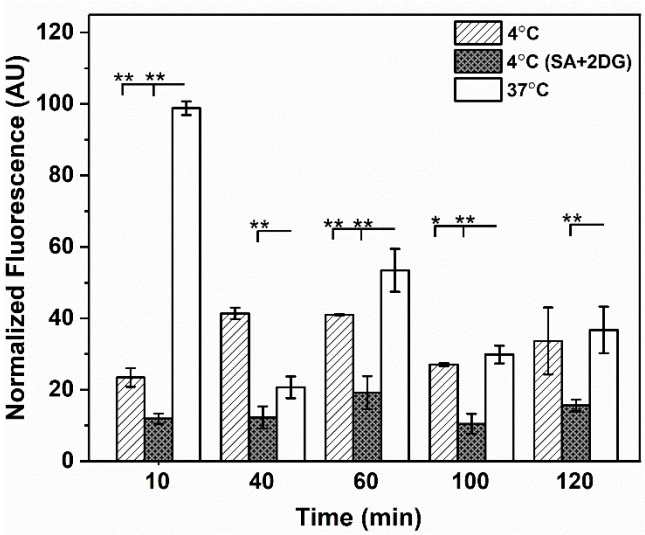

Fig* 5. *Characterization of D-chirality CPP uptake mechanism in HeLa cells. *Intact HeLa cells were pretreated under different conditions for 2 h before experimentation. Energy-dependent conditions were tested here to understand the role of endocytosis in peptide internalization. Uptake at control 37°C was compared with 4°C and 4°C in the presence of endocytosis inhibitors, 10 mM sodium azide (SA) + 5mM 2-deoxyglucose (2DG). (A) Cellular uptake in the presence of endocytosis inhibitors at 4°C drastically decreased when compared to control 37°C. *denotes* $p < 0.05$ *and **denotes* $p < 0.001$ *denotes statistical significance of decreased D-rwrwr uptake in the presence of endocytosis inhibitors when compared to control. All data are representative of duplicate experiments with each data point performed in triplicate to produce the error bars.*

endocytosis-inhibited condition at 4°C, there was a lag of ~30 min in attaining a saturated concentration with an observed pseudo steady state occurring after 60 min. It is interesting to note that despite a ~2.5-fold decrease in maximum cellular concentration at 4°C, the steady state internalization time was same as cells incubated with D-chirality CPPs at 37°C. This indicated that cellular uptake occurred via multiple mechanisms where inhibition of one uptake pathway resulted in peptide uptake via another mechanism. In the case of DS-rwrwr, peptide uptake occurred via direct penetration upon inhibition of endocytosis. This trend was similar in the presence of metabolic inhibitors; however, with a ~50 min lag time observed in attaining a saturated concentration. This led to an eventual pseudo steady state with a ~5-fold decrease in peptide uptake when compared to cells incubated with CPPs at 37°C. Fluorescence microscopy experiments were performed to further understand this mechanism of peptide uptake at 4°C in the presence of metabolic inhibitors (Supporting Information, Fig S4A). A punctate intracellular peptide distribution was observed in intact HeLa cells incubated with DS-rwrwr at 37°C after 10 min. This distribution was otherwise absent upon cellular inhibition of endocytosis. These small, distinct regions found in cells incubated at 37°C depict the intracellular trafficking occurring during endocytosis. CPPs taken in via endocytosis can get entrapped in early endosome vesicles leading to the formation of late endosomes and finally transported to lysosomes. The results from the microscopy studies clearly show that D-chirality CPP uptake is energy dependent; however, a heterogeneous cytosolic and nucleic distribution of DS-rwrwr was observed in cells incubated at 37°C alongside the punctate distribution. This suggested that D-chirality CPP uptake was energy dependent only to a certain degree and was not an absolute requirement for successful internalization. As expected, a uniform cytosolic distribution was observed under endocytosis inhibition demonstrating a possible direct diffusion of CPPs into cells. This trend was observed at

incubation times up to 120 min (Supporting Information, Fig S4B), proving that direct penetration is the limiting mechanism for D-chirality CPP uptake.

Peptide Export Occurs via an Exocytosis Independent Manner with Measurable CPP Levels Maintained within the Cytosol. Until this point, D-chirality CPP uptake was measured by

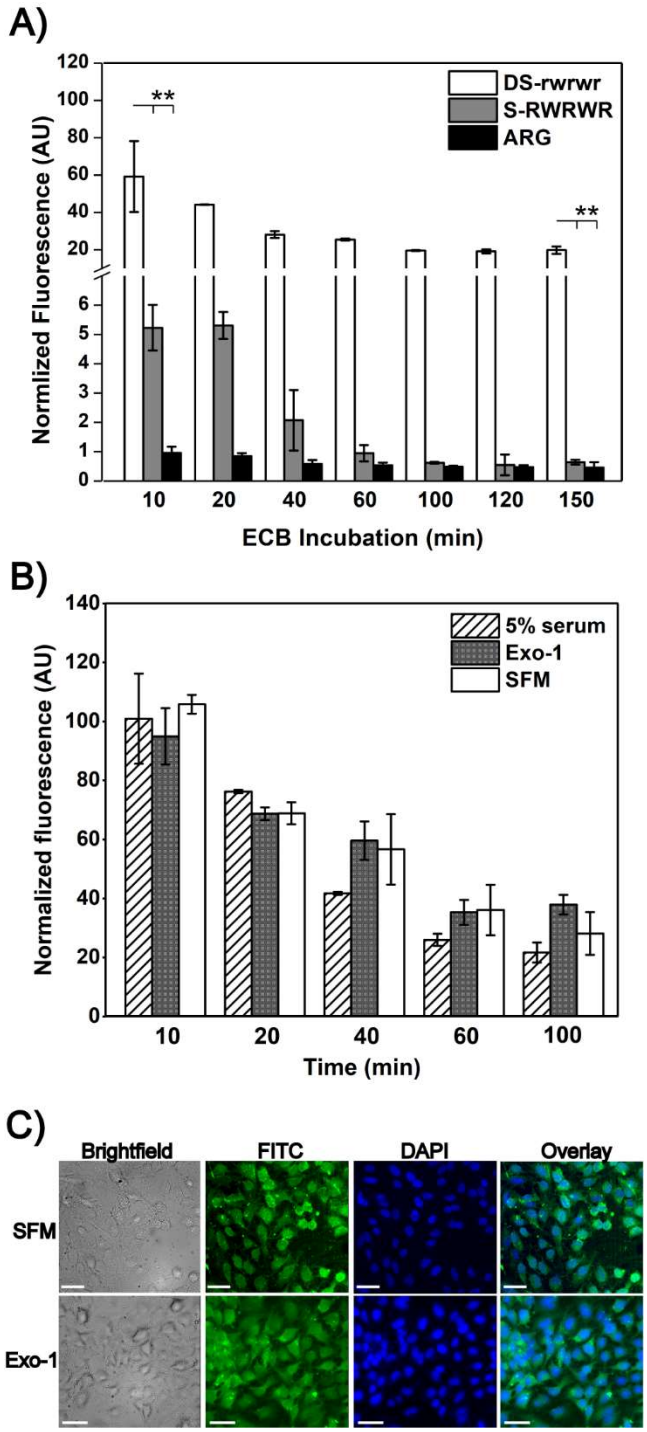

Fig 6. Characterization of export mechanism of D-CPPs in HeLa cells upon maximum internalization. *Intact HeLa cells were directly incubated with 10 µM of DS-rwrwr, S-RWRWR and ARG for 10 min in (A), while pretreated at respective conditions for 2 h and then incubated with 10 µM of DS-rwrwr for 10 min in (B) and (C), followed by washing and lysing cells for fluorometric or staining for fluorescence microscopy analysis. (A) Time dependent measurements of intracellular content of DS-rwrwr, S-RWRWR and ARG. Data demonstrates significant retention of DS-rwrwr within cells beyond 150 min, as well as increased intracellular signals against S-RWRWR and ARG. **denotes $p < 0.001$. (B) Effect of serum (exocytosis enhancer) and Exo-1 (exocytosis inhibitor) on exocytosis. Data suggests an insignificant difference in peptide retention in these populations ($p > 0.05$). (C) Characterization of exocytosis of DS-rwrwr from intact HeLa cells. Upon washing, cells were fixed with 4% PFA for 10 min and stained with 8 µM Hoechst 3342 nucleic acid staining for 30 min in the dark. Fluorescence FITC channel highlights the presence of DS-RWRWR and its uniform intracellular distribution after 150 min, while DAPI shows the cellular nuclei. All scale bars are 50 µm.*

experimentation using a constant, exogenous peptide concentration. Results from these experiments suggested that a saturated intracellular concentration occurred within 10 min after which a pseudo steady state was attained for peptide internalization. An oscillatory trend was observed for cells incubated at longer time periods; however, it was unclear what caused this increase and decrease of total peptide inside of cells since the data indicated that the D-chirality CPPs were highly stable under intracellular conditions (Fig 1C). To address this question, additional experiments were performed to investigate the possibility of CPP expulsion via exocytosis. HeLa cells were incubated with DS-rwrwr for 10 min then followed by the removal of the exogenous peptide solution and its replacement with ECB. A time-dependent analysis showed a decrease in internalized CPP levels until 100 min that reached a constant value after 120 min (Fig 6A). Statistical analysis comparing the intracellular fluorescence at different time points proved that there was a significant decrease in intracellular fluorescence between 10 min and 100 min. While considering the stability of DS-rwrwr and the minimal degradation in the presence of proteases (Fig 1C), these results suggested that a proportion of intact CPP were expelled from cells thus leading to a decrease in intracellular fluorescence levels. Parallel analysis from Fig 6A revealed that despite a certain level of expulsion, DS-rwrwr was retained to a greater extent than S-RWRWR and ARG (~20-folds higher, $p<0.001$).

Exocytosis was hypothesized to be the mode of peptide export since D-CPP uptake was, in part, controlled by endocytosis. Several recent works have highlighted that exocytosis was a predominant export mechanism in cells with a significant endocytosis mode of entry. One such study by Chu et al. showed that clusters of silica NPs in lysosomes are more easily exocytosed compared to NPs that are in cytosol.[39] An exocytosis inhibition experiment was performed where a population of cells were treated with the exocytosis inhibitor Exo-1. Exo-1 is a well-

known reversible inhibitor of vesicular trafficking between endoplasmic reticulum and the Golgi apparatus.[40] Blocking the exocytosis pathway with Exo-1 can help retain a significant amount of intracellular peptide within late endosomal vesicles. In parallel, a second population was treated with 5% serum, since rate of exocytosis has been shown to increase in the presence of serum. These two populations were compared against a control population of cells that were exposed to the CPPs in serum free media. Results from these experiments showed that neither Exo-1 nor serum affected cellular exocytosis (Fig 6B). Statistical analysis revealed that intracellular fluorescence in all three conditions (serum free media, Exo-1, serum) remained identical but decreased over time ($p>0.05$, Supporting Information, Table S4), suggesting that peptide export did not occur via exocytosis but through a direct escape similar in behavior to direct translocation. To visually confirm this hypothesis, fluorescence microscopy experiments were performed in intact HeLa cells in both serum free and inhibited exocytosis conditions. Fig 6C shows a uniform cytosolic distribution of DS-rwrwr, but punctate fluorescence regions after 150 min in the presence and absence of Exo-1 highlighting that inhibition of exocytosis did not have any effect in the intracellular levels of peptide. These findings confirmed that both uptake and export of D-chirality CPPs occurred via an energy independent direct penetration in and out of the cells. Despite being expelled through direct penetration out of cells, a measurable cytosolic level of DS-rwrwr can be seen in Fig 6C.

Characterization of D-chirality CPP Uptake and Export Kinetics. Empirical uptake and export characterization results clearly show that D-chirality CPP uptake occurred via both direct penetration and endocytosis and once internalized, both degraded peptide fragments and intact peptide get exported out of cells with a measurable intracellular CPP level. Besides intrinsic properties of CPPs, uptake is also influenced by cell type and its membrane composition thus,

making peptide internalization a complex multi-step process. Based on current results of this work

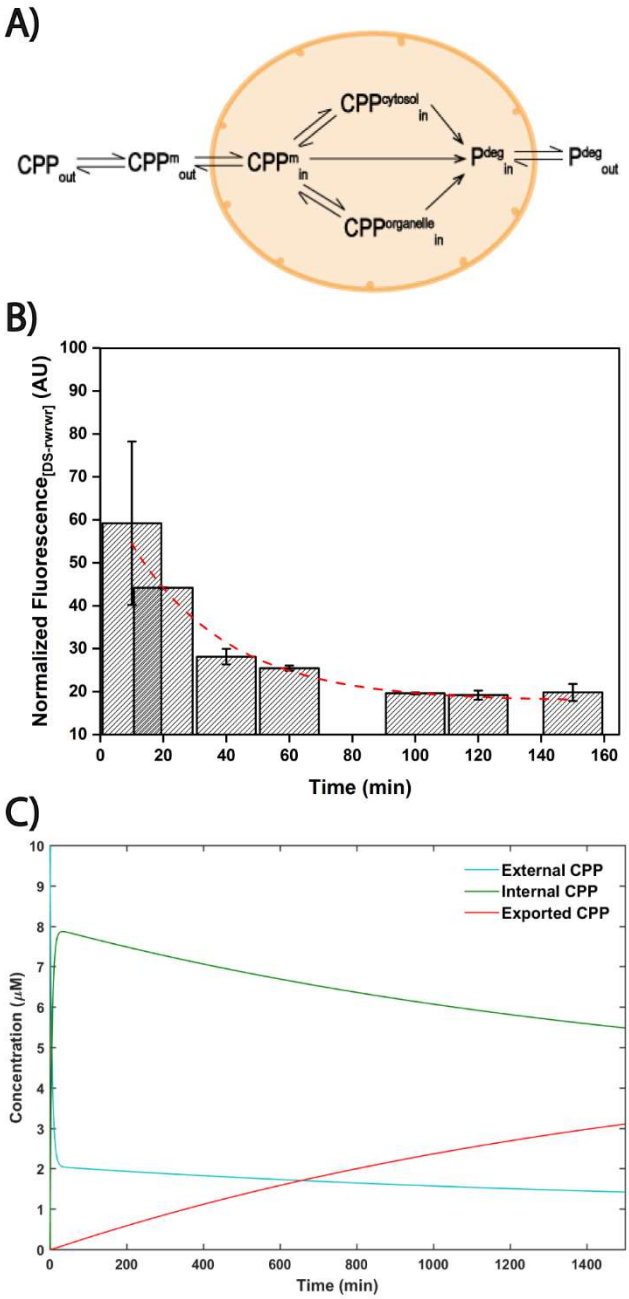

Fig 7. Kinetic model for D-chirality uptake and export. *A) Scheme representing equilibrated (uptake and export) and non-equilibrated (degradation) steps. CPP is cell-penetrating peptide and* P^{deg} *is degradation product, m denotes membrane bound CPP, label cytosol is for CPP present freely in the cytosol and label organelle is the CPP bound to the intracellular organelles. In and out represent the proportion of CPP or its degraded products inside and outside of cell. Numerical curve fitting of data points from export experiment shown by bar plot in B). Non-linear regression analysis (trendline in red dashes) yields an export rate constant* $k_{out,1}$ *=0.0329±0.003* min^{-1}*,* r^2*>0.99. D) Mathematical modeling of CPP uptake and export kinetics using the calculated rate constants over a span of 24 h demonstrates a relationship between the external, internal and exported concentrations of CPP as shown in cyan, green and red.*

and several postulated processes in literature, a kinetic scheme (Fig 7A) was constructed consisting of equilibrated states (uptake and export) as well as non-equilibrated steps (degradation).[41-43] While the amount of internalized CPP can be easily determined empirically, it is extremely difficult to measure membrane bound CPP and the separate fractions that are free in cytosol and are bound inside organelles. Modeling the complete scheme required a large number of assumptions and approximations making it an extremely unreliable model. To simplify things, a reduced model (Supplementary Information, Mathematical Modeling, Equation (S5)) was used to approximate the uptake and export kinetics.

Numerical treatment of the experimental DS-rwrwr internalization (Fig 2A) and subsequent non-linear regression analysis (Supplementary Information, Fig S5A) determined a k_{int} value of 0.1546±0.09 min^{-1} with r^2=0.74 and a half time of internalization value ($t_{0.5}$) of 7.83 min. The lower r^2 was due to the relative unsteady internalization behavior found in the experimental data. This can be verified by running the experiment at different initial peptide concentrations to confirm that the internalization reaction follows a first order. Similarly, non-linear curve fitting of the degradation data (Fig 1C) resulted in Supplementary Information, Fig S5B with a k_{deg} value of 0.434±0.01 X 10^{-3} min^{-1} and r^2=0.88. The low rate constant value suggested that peptide degradation occurs at very slow rate and is the nonlimiting reaction. Such a low degradation rate constant denotes that there was almost no intracellular degraded peptide fragments ($CPP^{deg}_{in} << CPP_{intact}$) in $CPP^{total}_{in} = CPP_{intact} + CPP^{deg}_{in}$ and thus resulting in $CPP^{total}_{in} = CPP_{intact}$. For the export kinetics, a ($k_{out,1} + k_{out,2}$) value of 0.0329±0.003 min^{-1} was obtained with $r^2 > 0.99$ (Fig 7B). $k_{out,1}$ is the rate constant for the export of intact cells while $k_{out,2}$ is the rate constant for export of peptide fragments. Since DS-rwrwr was stable and its rate of degradation intracellularly was very low, $k_{out,2}$ was assumed to be negligible. Thus, the export rate constant was driven by the export of just

the intact peptide which simplifies to $k_{out,1}$ = 0.0329±0.003 min^{-1}. The equilibrium rate constant for intact peptide $K_{intact}=k_{int}/k_{-out,1}$ = 3.7734, suggesting a faster intact CPP uptake of over export, while the equilibrium rate constant for the degraded peptide was negligible due to a lower degradation rate. The higher equilibrium constant for intact peptide can be validated by the fast internalization and cellular saturation occurring within 10 min followed by a slow export. The obtained rate constants (k_{int}, k_{deg}, $k_{out,1}$, $k_{-out,}$, $k_{-out,2}$) were all utilized by Equation (S5) (Supplementary Information, Mathematical Modeling) to obtain a relationship between intracellular fluorescence and concentration by obtaining relevant concentration levels of [CPP^{total}_{in}], which is the total internal CPP concentration and [CPP_{out}], which is the total CPP exported out of cells in terms of μM (Fig 7C). A mathematical simulation was run for >1500 min with initial condition, at time t=0, [CPP_{ext}] = 10 μM. This was the initial condition used to generate the experimental data. From Fig 7C, a maximum internal CPP concentration was found to be 7.86 μM seen at 13.3 min (in green) after which it slowly decreased over time at a very slow steady rate to reach an internal CPP concentration of 5.45 μM at the end of 24 h. This decrease in the internal CPP concentration was due to the intact CPP being exported as shown in red in Fig 7C. The concentration of exported CPP increased at a slow rate and reached 3.14 μM at the end of 24 h. This highlights the ability of DS-rwrwr to be exported from cells in its intact form due to significant intracellular stability. The concentration of the external CPP (shown in blue in Fig 7C) decreased proportionally with the increased cellular uptake at 13.3 min and gradually decreased at a steady rate until it attained an equilibrium with the exported CPP. The model simulated that all the three values attained equilibrium at some point >24 h suggesting that once rapid internalization, further CPP uptake and export is a very slow process. Such a mathematical representation serves as a base

in understanding the intracellular interactions of DS-rwrwr and can further aid in utilizing this CPP by itself or with a cargo in any biosensing or therapeutic applications.

CONCLUSION

Results from previous studies with β-hairpin secondary structured CPPs revealed a decreased uptake efficiency despite enhanced intracellular stability. Thus, in order to address this trade-off, the previously reported L-chirality unstructured CPPs were used as model sequences here to explore the broader consequences of L-to-D-chirality stereochemical conversion in CPP performance through a series of time, concentration, temperature and energy dependent uptake and export studies. A ~3-fold increase in cellular uptake was observed with DS-rwrwr against its L-chirality counterpart, S-RWRWR with a slight alteration in the mode of entry. While majority of uptake happened via direct penetration, it was partially controlled by endocytosis followed by endosomal escape and cytosolic access. Moreover, this inversion of chirality provided increased protease resistance where the D-chirality CPP exhibited a $t_{1/2}$ of ~1550 min, a 50-fold increase in comparison to a $t_{1/2}$ of ~ 28 min for its L-chirality counterpart. A series of exocytosis studies revealed that there was a notable export of the intact peptide through a direct penetration mode out of the cells. Additionally, even though the D-chirality peptide was found to be retained in the cytosol for several hours, it was found to be relatively innocuous to cells thus demonstrating its compatibility with cells under long exposure times. Finally, a theoretical uptake, reaction and export model was developed by numerically treating experimental data. The mathematical model predicted that for an initial 10 μM peptide solution concentration, maximum internalization of 7.86 μM occurred at 13.3 min followed by a pseudo-steady state decrease to 5.45 μM after 24 hours. As the internal CPP concentration increased, the CPP export increased at a slow rate to 3.14 μM after 24 h thus finally attaining equilibrium with internal CPP concentration at some point beyond 24 h. Such predictive reaction models help in better kinetic characterization of these CPPs when

designing therapeutics or when incorporated with cargoes. Altogether, the empirical results and theoretical models in this work establishes connections between chirality, cellular penetration, protease resistance, and intracellular activity that would be extremely useful for the development of future delivery agents with improved properties.

AUTHOR INFORMATION

Corresponding Author

*A.T.M.: Phone: +1 (225)-578-3062. E-mail: melvin@lsu.edu

Present Addresses

[1]Wilson Sonsini Goodrich & Rosati, 650 Page Mill Rd, Palo Alto, California 94304, United States

[2]ExxonMobil, 4999 Scenic Hwy, Baton Rouge, Louisiana 70802, United States

[3]Pfizer Inc., 875 Chesterfield Pkwy W, Chesterfield, Missouri 63017, United States

ACKNOWLEDGMENT

This work was supported by grants from the National Institute of Biomedical Imaging and Bioengineering, R03EB02935 (ATM), the National Science Foundation: CBET1509713 (ATM), and CBET1846900 (ATM), and the Louisiana Board of Regents, LEQSF(2018-23)-GF (HCH). The authors would like to thank Dong Liu (LSU AgCenter) for assistance with peptide synthesis, Joel T. Folse and Christopher Q. Ferrier (LSU Chemical Engineering) for some assistance with experiments.

CONFLICT OF INTEREST

The authors declare no conflict of interest

REFERENCES

1. Langel Ü. *CPP, CELL-PENETRATING PEPTIDES*: Springer, 2019.
2. Böhmová E, Machova D, Pechar M, et al. Cell-Penetrating Peptides: a Useful Tool for the Delivery of Various Cargoes Into Cells. Physiological research 2018;**67**:S267-S79
3. Copolovici DM, Langel K, Eriste E, Langel U. Cell-penetrating peptides: design, synthesis, and applications. ACS nano 2014;**8**(3):1972-94
4. Milletti F. Cell-penetrating peptides: classes, origin, and current landscape. Drug discovery today 2012;**17**(15-16):850-60
5. Zou Y, Ma D, Wang Y. The PROTAC technology in drug development. Cell biochemistry and function 2019;**37**(1):21-30
6. Jiang Y, Deng Q, Zhao H, et al. Development of stabilized peptide-based PROTACs against estrogen receptor α. ACS chemical biology 2017;**13**(3):628-35
7. Lu M, Liu T, Jiao Q, et al. Discovery of a Keap1-dependent peptide PROTAC to knockdown Tau by ubiquitination-proteasome degradation pathway. European journal of medicinal chemistry 2018;**146**:251-59

8. Gui W, Ott CA, Yang K, Chung JS, Shen S, Zhuang Z. Cell-permeable activity-based ubiquitin probes enable intracellular profiling of human deubiquitinases. J. Am. Chem. Soc 2018;**140**(39):12424-33
9. Safa N, Pettigrew JH, Gauthier TJ, Melvin AT. Direct measurement of deubiquitinating enzyme activity in intact cells using a protease-resistant, cell-permeable, peptide-based reporter. Biochemical Engineering Journal 2019;**151**:107320
10. Ying L, Wang Q. Microfluidic chip-based technologies: emerging platforms for cancer diagnosis. BMC biotechnology 2013;**13**(1):76
11. Safa N, Vaithiyanathan M, Sombolestani S, Charles S, Melvin AT. Population-based analysis of cell-penetrating peptide uptake using a microfluidic droplet trapping array. Analytical and Bioanalytical Chemistry 2019;**411**(12):2729-41 doi: 10.1007/s00216-019-01713-5[published Online First: Epub Date]|.
12. Zhang H, Curreli F, Waheed AA, et al. Dual-acting stapled peptides target both HIV-1 entry and assembly. Retrovirology 2013;**10**(1):136
13. Palm C, Jayamanne M, Kjellander M, Hällbrink M. Peptide degradation is a critical determinant for cell-penetrating peptide uptake. Biochimica et Biophysica Acta (BBA)-Biomembranes 2007;**1768**(7):1769-76
14. Skwarczynski M, Toth I. Cell-penetrating peptides in vaccine delivery: facts, challenges and perspectives: Future Science, 2019.
15. Keller A-A, Mussbach F, Breitling R, et al. Relationships between cargo, cell penetrating peptides and cell type for uptake of non-covalent complexes into live cells. Pharmaceuticals 2013;**6**(2):184-203
16. Song J, Qian Z, Sahni A, Chen K, Pei D. Cyclic Cell-Penetrating Peptides with Single Hydrophobic Groups. Chembiochem: a European journal of chemical biology 2019;**20**(16):2085-88
17. Borrelli A, Tornesello AL, Tornesello ML, Buonaguro FM. Cell penetrating peptides as molecular carriers for anti-cancer agents. Molecules 2018;**23**(2):295
18. Safa N, Anderson JC, Vaithiyanathan M, et al. CPProtectides: Rapid uptake of well-folded β-hairpin peptides with enhanced resistance to intracellular degradation. Peptide Science 2018:e24092
19. Agyei D, Danquah MK. Industrial-scale manufacturing of pharmaceutical-grade bioactive peptides. Biotechnology advances 2011;**29**(3):272-77
20. Traboulsi H, Larkin H, Bonin M-A, Volkov L, Lavoie CL, Marsault Er. Macrocyclic cell penetrating peptides: a study of structure-penetration properties. Bioconjugate chemistry 2015;**26**(3):405-11
21. Najjar K, Erazo-Oliveras A, Brock DJ, Wang T-Y, Pellois J-P. An l-to d-amino acid conversion in an endosomolytic analog of the cell-penetrating peptide TAT influences proteolytic stability, endocytic uptake, and endosomal escape. Journal of biological chemistry 2017;**292**(3):847-61
22. Pujals S, Fernández-Carneado J, Ludevid MD, Giralt E. D-SAP: a new, noncytotoxic, and fully protease resistant cell-penetrating peptide. ChemMedChem: Chemistry Enabling Drug Discovery 2008;**3**(2):296-301
23. Ramaker K, Henkel M, Krause T, Röckendorf N, Frey A. Cell penetrating peptides: a comparative transport analysis for 474 sequence motifs. Drug delivery 2018;**25**(1):928-37
24. Verdurmen WP, Bovee-Geurts PH, Wadhwani P, et al. Preferential uptake of L-versus D-amino acid cell-penetrating peptides in a cell type-dependent manner. Chemistry & biology 2011;**18**(8):1000-10

25. Elmquist A, Hansen M, Langel Ü. Structure–activity relationship study of the cell-penetrating peptide pVEC. Biochimica et Biophysica Acta (BBA)-Biomembranes 2006;**1758**(6):721-29
26. Nakase I, Konishi Y, Ueda M, Saji H, Futaki S. Accumulation of arginine-rich cell-penetrating peptides in tumors and the potential for anticancer drug delivery in vivo. Journal of controlled release 2012;**159**(2):181-88
27. Tamamura H, Kobayakawa T, Ohashi N. *Mid-size Drugs Based on Peptides and Peptidomimetics: A New Drug Category*: Springer, 2018.
28. Ngamdee K, Chaiendoo K, Saiyasombat C, et al. Highly selective circular dichroism sensor based on d-penicillamine/cysteamine-cadmium sulfide quantum dots for copper (II) ion detection. Spectrochimica Acta Part A: Molecular and Biomolecular Spectroscopy 2019;**211**:313-21
29. Brock R. The uptake of arginine-rich cell-penetrating peptides: putting the puzzle together. Bioconjugate chemistry 2014;**25**(5):863-68
30. Kumar P, Wu H, McBride JL, et al. Transvascular delivery of small interfering RNA to the central nervous system. Nature 2007;**448**(7149):39
31. Li Y, Zheng X, Cao Z, Xu W, Zhang J, Gong M. Self-assembled peptide (CADY-1) improved the clinical application of doxorubicin. Int. J. Pharm 2012;**434**(1-2):209-14
32. Smith PJ, Giroud M, Wiggins HL, et al. Cellular entry of nanoparticles via serum sensitive clathrin-mediated endocytosis, and plasma membrane permeabilization. International journal of nanomedicine 2012;**7**:2045
33. Ruseska I, Zimmer A. Internalization mechanisms of cell-penetrating peptides. Beilstein Journal of Nanotechnology 2020;**11**(1):101-23
34. Badkas A, Frank E, Zhou Z, et al. Modulation of in vitro phagocytic uptake and immunogenicity potential of modified Herceptin®-conjugated PLGA-PEG nanoparticles for drug delivery. Colloids and Surfaces B: Biointerfaces 2018;**162**:271-78
35. Mosquera Js, García I, Liz-Marzán LM. Cellular uptake of nanoparticles versus small molecules: a matter of size. Accounts of chemical research 2018;**51**(9):2305-13
36. Holm T, Andaloussi SE, Langel Ü. Comparison of CPP uptake methods. Cell-Penetrating Peptides: Springer, 2011:207-17.
37. Patel SG, Sayers EJ, He L, et al. Cell-penetrating peptide sequence and modification dependent uptake and subcellular distribution of green florescent protein in different cell lines. Scientific reports 2019;**9**(1):6298
38. Yu W, Zhan Y, Xue B, et al. Highly efficient cellular uptake of a cell-penetrating peptide (CPP) derived from the capsid protein of porcine circovirus type 2. Journal of Biological Chemistry 2018;**293**(39):15221-32
39. Chu Z, Huang Y, Tao Q, Li Q. Cellular uptake, evolution, and excretion of silica nanoparticles in human cells. Nanoscale 2011;**3**(8):3291-99
40. von Kleist L, Haucke V. At the crossroads of chemistry and cell biology: inhibiting membrane traffic by small molecules. Traffic 2012;**13**(4):495-504
41. Gao X, Hong S, Liu Z, Yue T, Dobnikar J, Zhang X. Membrane potential drives direct translocation of cell-penetrating peptides. Nanoscale 2019;**11**(4):1949-58
42. Bechara C, Sagan S. Cell-penetrating peptides: 20 years later, where do we stand? FEBS letters 2013;**587**(12):1693-702
43. Guidotti G, Brambilla L, Rossi D. Cell-penetrating peptides: from basic research to clinics. Trends in pharmacological sciences 2017;**38**(4):406-24

SUPPORTING INFORMATION

Additional supporting information may be found online in the Supporting Information section at the end of the article.